Predominant magnetic states in the Hubbard model on anisotropic triangular lattices

T. Watanabe,[1,2] H. Yokoyama,[3] Y. Tanaka,[1,2] and J. Inoue[1]
[1]*Department of Applied Physics, Nagoya University, Nagoya 464-8603, Japan*
[2]*Core Research for Evolutional Science and Technology, Japan Science and Technology Cooperation, Japan*
[3]*Department of Physics, Tohoku University, Sendai 980-8578, Japan*
(Received 5 March 2008; published 5 June 2008)

By using an optimization variational Monte Carlo method, we study the half-filled-band Hubbard model on anisotropic triangular lattices, as a continuation of the preceding study [T. Watanabe, H. Yokoyama, Y. Tanaka, and J. Inoue, J. Phys. Soc. Jpn. **75**, 074707 (2006)]. We introduce two new trial states: (i) A coexisting state of Ψ_Q^{co}-antiferromagnetic (AF) and a *d*-wave singlet gaps, in which we allow for a band renormalization effect, and (ii) a state with an AF order of 120° spin structure. In both states, a first-order metal-to-insulator transition occurs at smaller U/t than that of the pure *d*-wave state. In insulating regimes, magnetic orders always exist; an ordinary (π,π)-AF order survives up to $t'/t\sim 0.9$ $(U/t=12)$, and a 120°-AF order becomes dominant for t'/t. The regimes of the robust superconductor and of the nonmagnetic insulator the preceding study proposed give way to these magnetic domains.

DOI: 10.1103/PhysRevB.77.214505 PACS number(s): 74.70.−b, 74.20.−z

I. INTRODUCTION

A series of κ-$(\mathrm{BEDT\text{-}TTF})_2X$ [κ-ET salts] have intriguing properties specific to strongly-correlated systems; they often undergo unconventional superconductor (SC)-to-insulator transitions through the chemical substitution of *X* or under applied pressure, and have good two-dimensionality in conductivity with frustrated lattice structure. As a model of these compounds, the half-filled-band Hubbard model on anisotropic triangular lattices[1] (an extended square lattice with hopping integral *t* in *x* and *y* directions, and t' in one diagonal direction [1,1]) has been intensively studied:[2]

$$\mathcal{H}=\sum_{\mathbf{k}\sigma}\varepsilon_{\mathbf{k}}c_{\mathbf{k}\sigma}^{\dagger}c_{\mathbf{k}\sigma}+U\sum_{i}n_{i\uparrow}n_{i\downarrow}, \tag{1}$$

where $t'/t\to 0$ and $t<t'<t'_{c2}$. To clarify the properties of this model in the strongly correlated region, $U/t\gg 1$, especially Mott transitions, reliable theoretical approaches are needed. To this end, the present authors recently applied to Eq. (1) an optimization (or correlated) variational Monte Carlo (VMC) method, which can deal with SC and a Mott transition as a continuous function of U/t. Henceforth, we call this preceding study "(I)."[3] In (I), we chiefly considered various properties of the $d_{x^2-y^2}$-wave singlet state, Ψ_Q^d, and constructed a ground-state phase diagram in the t'-U plane by comparing its energy with that of the ordinary (π,π)-antiferromagnetic (AF) state, Ψ_Q^{AF}. Most of the results are consistent with the behavior of κ-ET salts, but the area of an (π,π)-AF insulator is unexpectedly limited $t'/t=1$ in considering the appearance of the AF order, e.g., κ-$(\mathrm{ET})_2\mathrm{CuN}(\mathrm{CN})_2\mathrm{Cl}$ $E_{t'}/t$, as well as the vanishing point of the AF order expected in the J-J' Heisenberg model $(t'/t\sim 0.8)$.[4] As we pointed out in (I), this disagreement possibly stems from the fact that the *d*-wave singlet state and the AF state were treated separately; thereby, the former state does not include a seed of an AF long-range order and the latter a band renormalization effect.

For E_t/t, many theoretical studies[5–9] for the Hubbard model have obtained results of dominant nonmagnetic insulating state, which are consistent with the insulating state found in κ-$(\mathrm{ET})_2\mathrm{Cu}_2(\mathrm{CN})_3$ with Ψ_Q^{120}.[10] Nonetheless, we should be also concerned about the AF order with 120-degree spin structure, which is considered to prevail in the isotropic case of the $(U/t=12)$ Heisenberg model.[4,11] Actually, a recent VMC study[12] for a *t*-*J*-type model on the isotropic triangular lattice concluded that the 120°-AF ordered state is dominant in an unexpectedly wide range of doping rate. Thus, it is possible that the 120°-AF order is robust also in the Hubbard model with $t'\sim t$ and sufficiently small values of U/t for the organics.

In this paper, as a continuation of (I), we introduce two trial states: (i) A state which includes (π,π)-AF and *d*-wave gaps simultaneously;[13,14] and then a band (or Fermi-surface) renormalization effect, owing to the electron correlation is taken into account.[15] (ii) A state which exhibits the 120°-AF order. In addition to these functions, we newly consider SC states with pairing symmetries suitable for (d). Our main interest here is the competition among these states and those treated in (I). It is found that first-order metal-to-insulator transitions always occur at smaller values of U/t than those for the pure *d*-wave state. In the insulating regime, the (π,π)-AF order remains up to 120°, owing to the band renormalization effect we considered in the coexisting state, and the 120°-AF order becomes predominant in the range of $t'/t\gtrsim 0.9$. Consequently, a magnetic order, namely the (π,π)-AF or 120°-AF order, always exists in the insulating regime, and a regime of a nonmagnetic insulator vanishes. In addition, a domain of dominant SC found in (I) disappears within the present results. The previous phase diagram is substantially modified.

In Sec. II, we explain the trial wave functions used, and recapitulate the main points of (I) as a motivation of this study. In Sec III, we represent the VMC results. In Sec. IV, we briefly summarize this study, and compare to experimental and other theoretical results.

A part of the results have been reported before.[16]

II. WAVE FUNCTIONS

As usual, we use Jastrow-type trial wave functions, $\Psi = \mathcal{P}\Phi$, in which Φ denotes a one-body (Hartree–Fock) part expressed as a Slater determinant and $\mathcal{P}$ a many-body correlation factor. In Sec. II A, we describe the correlation factor $\mathcal{P}$. In Sec. II B, we point out insufficient points in the wave functions used in (I) and introduce a coexisting state of the (π,π)-AF and d-wave gaps, in which the one-body band structure is modified by optimizing a hopping parameter $\tilde{t}'$, as renormalization owing to electron correlation. In Sec. II C, we formulate a state with an AF order of 120° spin structure as another new trial state. In Sec. II D, we briefly touch on the conditions of the VMC calculations.

A. Correlation factor

When one treats the Hubbard model on the basis of a variational method, it is crucial to introduce, in addition to the well-known Gutzwiller (onsite) factor $\mathcal{P}_G$,[17,18] intersite correlation factors[19,20] into Jastrow-type wave functions. In particular, near half filling, the binding effect of a doubly occupied site (doublon) to an empty site (holon) is indispensable to describe a Mott transition, as well as various quantities appropriately.[19] To this end, we have repeatedly studied[3,21–23] a four-body factor formally written as

$$\mathcal{P}_Q = \prod_i (1 - \mu Q_i^{\tau})(1 - \mu' Q_i^{\tau'}), \tag{2}$$

$$Q_i^{\tau(\tau')} = \prod_{\tau(\tau')} [d_i(1 - e_{i+\tau(\tau')}) + e_i(1 - d_{i+\tau(\tau')})], \tag{3}$$

in which $d_i = n_{i\uparrow}n_{i\downarrow}$, $e_i = (1-n_{i\uparrow})(1-n_{i\downarrow})$, and τ (τ') run over all the adjacent sites in the bond directions of t (t'). In Eq. (2), μ (μ') is a variational parameter, which controls the binding strength between a doublon and a holon in the bond direction t (t'). We have confirmed that $\mathcal{P}_Q$ works effectively in the model, Eq. (1).[3]

B. Coexisting state of *d* wave and AF gaps

By using $\mathcal{P} = \mathcal{P}_Q\mathcal{P}_G$, we mainly studied, in (I), a $d_{x^2-y^2}$-wave singlet state: $\Psi_Q^d = \mathcal{P}\Phi_d$, where Φ_d is the BCS function with a $d_{x^2-y^2}$-wave gap:

$$\Delta_{\mathbf{k}} = \Delta_d(\cos k_x - \cos k_y). \tag{4}$$

In Ψ_Q^d, we allow for renormalization of the one-body band $\varepsilon_{\mathbf{k}}$, owing to electron correlation by varying $t'(\equiv\tilde{t}')$ in Φ_d as a variational parameter,[15] independently of t' fixed in the Hamiltonian Eq. (1). In (I), we obtained the following results within Ψ_Q^d. (i) A first-order Mott (conductor-to-nonmagnetic-insulator) transition takes place for arbitrary t'/t at $U = U_c$ roughly of the bandwidth. This transition is induced by the binding (and unbinding) of a doublon (negatively charged) to a holon (positively charged) unlike the famous Brinkman–Rice transition.[24] (ii) Robust d-wave SC appears in a restricted parameter range immediately below U_c and of weak frustration ($t'/t \lesssim 0.7$). This SC is considered to be induced by a short-range (π,π)-AF spin correlation because whenever the superconducting (SC) correlation function is sizably enhanced, the spin structure factor $S(\mathbf{q})$ has a sharp peak at the AF wave number, $\mathbf{q} = \mathbf{K} = (\pi,\pi)$. (iii) In the insulating regime, Ψ_Q^d exhibits a spin-gap behavior and does not have a (π,π)-AF long-range order, although $S(\mathbf{q})$ has a sharp peak at $\mathbf{q} = \mathbf{K}$, namely a short-range AF correlation considerably develops.

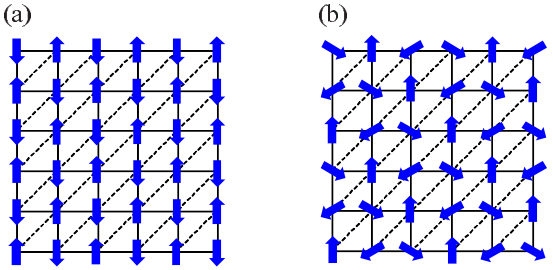

FIG. 1. (Color online) Schematic representation of spin structure in two AF orders studied in this paper for the anisotropic triangular lattice: (a) an ordinary (π,π)-AF order and (b) an AF order with 120° spin structure.

To consider the competition between Ψ_Q^d and a state with the (π,π)-AF long-range order [see Fig. 1(a)], which should prevail for small t'/t, we also studied a projected AF state, $\Psi_Q^{\mathrm{AF}} = \mathcal{P}\Phi_{\mathrm{AF}}$, where Φ_{AF} is a mean-field-type (π,π)-AF state. In Ψ_Q^{AF}, we did not renormalize $\tilde{t}'$, because the variational energy E to be minimized becomes a discrete function of $\tilde{t}'/t$. We found that (iv) the stable range of Ψ_Q^{AF} against Ψ_Q^d is restricted to a weakly frustrated regime, $t'/t \lesssim 0.4$ (for $U/t = 6$), and this range tends to shrink as U/t increases. As notified in (I), the above results (iii) and (iv) are not consistent with various approximate results[4] for the corresponding J-J' spin model, which predict that the (π,π)-AF domain continues up to $t'/t \sim 0.8$. To resolve this disagreement, a seed of the AF order should be introduced into Ψ_Q^d and the renormalization of $\varepsilon_{\mathbf{k}}$ owing to U into Ψ_Q^{AF}.

In this paper, we study a wave function, $\Psi_Q^{\mathrm{co}} = \mathcal{P}\Phi_{\mathrm{co}}$, which meets the above requirements by merging Ψ_Q^d and Ψ_Q^{AF}. In Ψ_Q^{co}, the d-wave gap and an AF order can coexist.[13] The one-body part is written as

$$\Phi_{\mathrm{co}} = \left(\sum_{\mathbf{k}} \varphi_{\mathbf{k}} b_{\mathbf{k},\uparrow}^{\dagger} b_{-k,\downarrow}^{\dagger}\right)^{N_e/2} |0\rangle, \tag{5}$$

in which N_e is the electron number, and $\varphi_{\mathbf{k}}$ is the ratio of BCS coefficients:

$$\varphi_{\mathbf{k}} = \frac{v_{\mathbf{k}}}{u_{\mathbf{k}}} = \frac{\Delta_{\mathbf{k}}}{\tilde{\varepsilon}_{\mathbf{k}} - \zeta + \sqrt{(\tilde{\varepsilon}_{\mathbf{k}} - \zeta)^2 + \Delta_{\mathbf{k}}^2}}, \tag{6}$$

with

$$\tilde{\varepsilon}_{\mathbf{k}} = -2t(\cos k_x + \cos k_y) - 2\tilde{t}' \cos(k_x + k_y), \tag{7}$$

and $b^{\dagger}$ is a creation operator that diagonalizes the ordinary (π,π)-AF Hartree–Fock Hamiltonian, and is given as

$$b_{\mathbf{k},\sigma}^{\dagger} = \alpha_{\mathbf{k}} c_{\mathbf{k},\sigma}^{\dagger} + s\beta_{\mathbf{k}} c_{\mathbf{k}+\mathbf{K},\sigma}^{\dagger}, \tag{8}$$

$$b_{\mathbf{k}+K,\sigma}^{\dagger} = -s\beta_{\mathbf{k}} c_{\mathbf{k},\sigma}^{\dagger} + \alpha_{\mathbf{k}} c_{\mathbf{k}+\mathbf{K},\sigma}^{\dagger}, \tag{9}$$

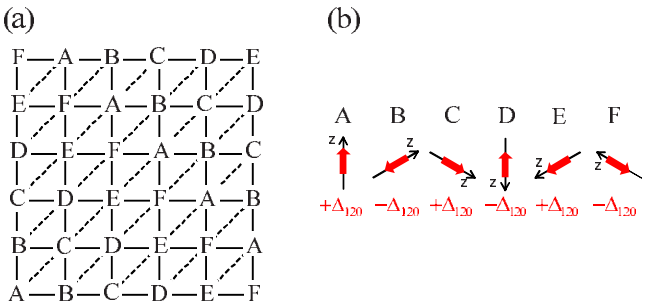

FIG. 2. (Color online) Schematic explanation of Hartree–Fock approximation for an AF order with 120° spin structure. In (a), it is shown how we divide the anisotropic triangular lattice into six sublattices (*A*-*F*) with different directions of a spin quantization axis, which are illustrated in (b): the axis of B (C,D,E,F,A) sublattice is obtained by turning that of A (B,C,D,E,F) sublattice by 60 degrees. For these sublattices, we suppose that the gap parameter is staggered, namely Δ_{120}, $-\Delta_{120}$, Δ_{120},$\cdots$, leading to the formation of a 120°-AF order in Fig. 1(b).

$$\alpha_{\mathbf{k}}(\beta_{\mathbf{k}}) = \sqrt{\frac{1}{2}\left(1 - (+)\frac{\gamma_{\mathbf{k}}}{\sqrt{\gamma_{\mathbf{k}}^2 + \Delta_{\mathrm{AF}}^2}}\right)}, \tag{10}$$

with $\gamma_{\mathbf{k}} = -2t(\cos k_x + \cos k_y)$ and $\varsigma = +(-)1$, accordingly as $\sigma = \uparrow$ ($\downarrow$). In addition to the six parameters in Ψ_Q^d, namely, g [Gutzwiller (onsite) parameter], μ, μ', Δ_d, ζ (chemical potential), and $\tilde{t}'$, Ψ_Q^{co} has the seventh parameter Δ_{AF}, which controls the staggered spin field and is closely connected to the (π,π)-AF order parameter m_s (sublattice magnetization). Note that, in contrast to Δ_{AF}, a finite optimized value of Δ_d does not necessarily mean that a SC gap opens, but an insulating spin gap. For $\Delta_{\mathrm{AF}}(\Delta_d) \to 0$, Ψ_Q^{co} is reduced to Ψ_Q^d (Ψ_Q^{AF}). Thus, we may regard Ψ_Q^{co} as Ψ_Q^d, in which the (π,π)-AF long-range order can arise, and also as Ψ_Q^{AF} into which a band renormalization effect is introduced through the *d*-wave gap.

C. AF-ordered state with 120-degree spin structure

As discussed in (I), an AF-ordered state with 120° spin structure [see Fig. 1(b)] is plausible for the region of $t'/t \sim 1$. We introduce such a state, $\Psi_{120} = \mathcal{P}\Phi_{120}$, for the Hubbard model Eq. (1) and check its stability for finite values of U/t and consistency with the results obtained for $U/t = \infty$.[4,11]

As the one-body part, Φ_{120}, we use a Hartree–Fock ground state for the Hamiltonian Eq. (1). As explained in Fig. 2, we consider six sublattices (A-F); the spin quantization axis of a sublattice is turned by 60 degrees from that of a neighboring sublattice. By using this scheme, the Hamiltonian Eq. (1) is transformed to

$$H = -\sum_{\lambda}\left[t\sum_{<i_\lambda, j_{\lambda+1}>}(a_{i_\lambda,\uparrow}^\dagger a_{i_\lambda,\downarrow}^\dagger)R\left(\frac{\pi}{6}\right)\begin{pmatrix} a_{j_{\lambda+1},\uparrow} \\ a_{j_{\lambda+1},\downarrow}\end{pmatrix} + t'\sum_{(i_\lambda, j_{\lambda+2})}(a_{i_\lambda,\uparrow}^\dagger a_{i_\lambda,\downarrow}^\dagger)R\left(\frac{\pi}{3}\right)\begin{pmatrix} a_{j_{\lambda+2},\uparrow} \\ a_{j_{\lambda+2},\downarrow}\end{pmatrix}\right] + \mathrm{H.c.} + U\sum_{\lambda}\sum_{i_\lambda} n_{i\uparrow}^T n_{i\downarrow}^T, \tag{11}$$

where

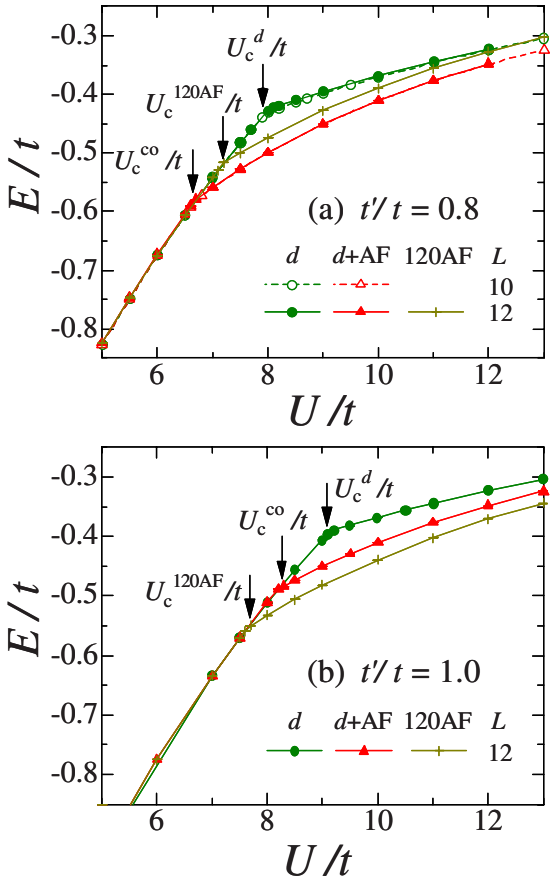

FIG. 3. (Color online) Total energies of the coexisting state Ψ_Q^{co} [d+AF], the 120°-AF state Ψ_Q^{120} [120 AF], and the *d*-wave state Ψ_Q^d [d] are compared as a function of the correlation strength for (a) $t'/t = 0.8$ and (b) 1.0. The critical values of Mott transitions U_c/t are indicated by arrows for respective states. Although the data for $L = 10$ and 12 are plotted, the system-size dependence is almost negligible in this scale. For $t'/t = 1$, the system of $L = 10$ is not used because the closed-shell condition is not satisfied.

$$R(\theta) = \begin{bmatrix} \cos(\theta) & -\sin(\theta) \\ \sin(\theta) & \cos(\theta) \end{bmatrix}, \tag{12}$$

$a_{i\sigma}^\dagger$ is a creation operator in the sublattice representation, $n_{i\sigma}^T = a_{i,\sigma}^\dagger a_{i,\sigma}$, λ (=*A*-*F*) is a sublattice index, i_λ runs over all the sites on sublattice λ, and an angle (round) bracket in the summation indices in Eq. (11) indicates a nearest (diagonal)-neighbor pair. We apply a Hartree–Fock decoupling to the interaction term in Eq. (11),

$$\sum_i U n_{i\uparrow}^T n_{i\downarrow}^T \sim \sum_i U(\langle n_{i\uparrow}^T\rangle n_{i\downarrow}^T + \langle n_{i\downarrow}^T\rangle n_{i\uparrow}^T) + \mathrm{const.}, \tag{13}$$

and assume that the gap is staggered as

$$\frac{U}{2}(\langle n_{i_\lambda\uparrow}^T\rangle - \langle n_{i_\lambda\downarrow}^T\rangle) \equiv \begin{cases} +\Delta_{120} & \text{if} \quad \lambda = A,C,E \\ -\Delta_{120} & \text{if} \quad \lambda = B,D,F \end{cases}, \tag{14}$$

to form a 120°-AF order. By using the operators for sublattices, the Hartree–Fock Hamiltonian in the wave-number representation is given as

$$H_{\mathrm{HF}} = \sum_{\mathbf{k},\sigma} (a^{\dagger A}_{\mathbf{k},\sigma} a^{\dagger B}_{\mathbf{k},\sigma} a^{\dagger C}_{\mathbf{k},\sigma} a^{\dagger D}_{\mathbf{k},\sigma} a^{\dagger E}_{\mathbf{k},\sigma} a^{\dagger F}_{\mathbf{k},\sigma}) \begin{pmatrix} -\sigma\Delta_{120} & A_1 & A_2^* & 0 & A_2 & A_1^* \\ A_1^* & \sigma\Delta_{120} & A_1 & A_2^* & 0 & A_2 \\ A_2 & A_1^* & -\sigma\Delta_{120} & A_1 & A_2^* & 0 \\ 0 & A_2 & A_1^* & \sigma\Delta_{120} & A_1 & A_2^* \\ A_2^* & 0 & A_2 & A_1^* & -\sigma\Delta_{120} & A_1 \\ A_1 & A_2^* & 0 & A_2 & A_1^* & \sigma\Delta_{120} \end{pmatrix} \begin{pmatrix} a^A_{\mathbf{k},\sigma} \\ a^B_{\mathbf{k},\sigma} \\ a^C_{\mathbf{k},\sigma} \\ a^D_{\mathbf{k},\sigma} \\ a^E_{\mathbf{k},\sigma} \\ a^F_{\mathbf{k},\sigma} \end{pmatrix}$$

$$+ \sum_{\mathbf{k}\sigma} (a^{\dagger A}_{\mathbf{k},\sigma} a^{\dagger B}_{\mathbf{k},\sigma} a^{\dagger C}_{\mathbf{k},\sigma} a^{\dagger D}_{\mathbf{k},\sigma} a^{\dagger E}_{\mathbf{k},\sigma} a^{\dagger F}_{\mathbf{k},\sigma}) \begin{pmatrix} 0 & B_{1+} & B_{2+} & 0 & B_{2-} & B_{1-} \\ B_{1-} & 0 & B_{1+} & B_{2+} & 0 & B_{2-} \\ B_{2-} & B_{1-} & 0 & B_{1+} & B_{2+} & 0 \\ 0 & B_{2-} & B_{1-} & 0 & B_{1+} & B_{2+} \\ B_{2+} & 0 & B_{2-} & B_{1-} & 0 & B_{1+} \\ B_{1+} & B_{2+} & 0 & B_{2-} & B_{1-} & 0 \end{pmatrix} \begin{pmatrix} a^A_{\mathbf{k},-\sigma} \\ a^B_{\mathbf{k},-\sigma} \\ a^C_{\mathbf{k},-\sigma} \\ a^D_{\mathbf{k},-\sigma} \\ a^E_{\mathbf{k},-\sigma} \\ a^F_{\mathbf{k},-\sigma} \end{pmatrix} + \text{const.}, \tag{15}$$

where $a^{\lambda\dagger}_{\mathbf{k},\sigma}$ is the Fourier transformation of $a^{\dagger}_{i\lambda,\sigma}$ and

$$A_1 = -t\cos(\pi/6)(e^{-ik_x} + e^{-ik_y}),$$

$$A_2 = -t'\cos(\pi/3)e^{-i(k_x+k_y)},$$

$$B_{1+} = t\sin(\pi/6)(e^{-ik_x} + e^{-ik_y}),$$

$$B_{1-} = -t\sin(\pi/6)(e^{ik_x} + e^{ik_y}),$$

$$B_{2+} = t'\sin(\pi/3)e^{-i(k_x+k_y)},$$

$$B_{2-} = -t'\sin(\pi/3)e^{i(k_x+k_y)}. \tag{16}$$

As Φ_{120}, we adopt the lowest-energy eigenvector obtained by diagonalizing Eq. (15). However, we do not determine Δ_{120} by a self-consistent equation in the Hartree–Fock approximation but optimize Δ_{120} as a variational parameter in Ψ_Q^{120} simultaneously with the other parameters with respect to the original Hamiltonian Eq. (11). If Δ_{120} is finite, all sublattices have staggered spin densities, constituting the 120° spin structure.

D. Variational Monte Carlo calculations

Generally, it is not easy to accurately calculate expectation values of a many-body wave function with analytic approaches. Here, we apply an optimization VMC method,[25] which effectively minimizes the variational energy and makes a virtually accurate evaluation, to the wave functions mentioned in this section. We have performed VMC calculations mainly for the lattice of $N_s = L \times L$ sites with $L=10$ and 12. The conditions of calculations here are mostly the same as those in (I).

III. RESULTS

In Sec. III A, we consider the energies of Ψ_Q^{co} and Ψ_Q^{120}, and the critical behaviors appearing in them. In Sec. III B, we show these critical behaviors indicate a metal-to-insulator transition. In Sec. III C, we discuss the properties of the AF order in the insulating regime of Ψ_Q^{co} and the eventual phase diagram. In Sec. III D, we consider the BCS state with other pairing symmetries expected for the region of $t' \gtrsim t$.

A. Stability of coexisting state and 120°-AF state

We start with the energy reduction of the coexisting state Ψ_Q^{co} and the 120°-AF state Ψ_Q^{120} for $t' \sim t$. In Figs. 3(a) and 3(b), the total energy per site E is compared among Ψ_Q^{co} (E^{co}), Ψ_Q^{120} (E^{120}), and Ψ_Q^{d} (E^{d}) for $t'/t=0.8$ and 1.0, respectively. For both values of t'/t, the curves of E/t for the three states are almost indistinguishable from one another for small U/t, whereas they separate with cusps as U/t becomes large. In fact, as we will see shortly, these cusps indicate metal-insulator transitions. For $t'/t=0.8$, E^{co} exhibits a cusp first at $U=U_c^{\mathrm{co}}=6.65t\pm0.05t$ and becomes appreciably lower than both E^d and E^{120} for $U>U_c^{\mathrm{co}}$. On the other hand, for $t'/t=1.0$, E^{120} exhibits a cusp first at $U=U_{\mathrm{c}}^{120}=7.65t\pm0.05t$ and becomes the lowest for $U>U_c^{120}$. Thus, the lowest-energy state for large U/t is switched from Ψ_Q^{co} to Ψ_Q^{120} in the range of $0.8<t'/t<1.0$. To see t'/t dependence of E/t in the insulating regime ($U>U_c$), we plot the total energies at $U/t=12$ of various states in Fig. 4. For $t'<t'_c \sim 0.90t$, the coexisting state is the most stable, and the decrease in E/t from E^d/t estimated in (I) is approximately 7.6%, irrespective of the value of t'/t. This invariant behavior of E/t with respect to t'/t is caused by marked band renormalization; this point will be discussed in detail in Sec. III C. In contrast, E^{120} decreases rapidly as t'/t increases and becomes the lowest for $t'>t'_{c1}$. As expected, Ψ_Q^{120} becomes predominant near the symmetric point ($t'/t\sim1$). Consequently, the area where the pure d-wave singlet state Ψ_Q^d prevails does not appear in the insulating regime.

To discuss the energy reduction more closely, especially in the conductive regime, we introduce the condensation energy

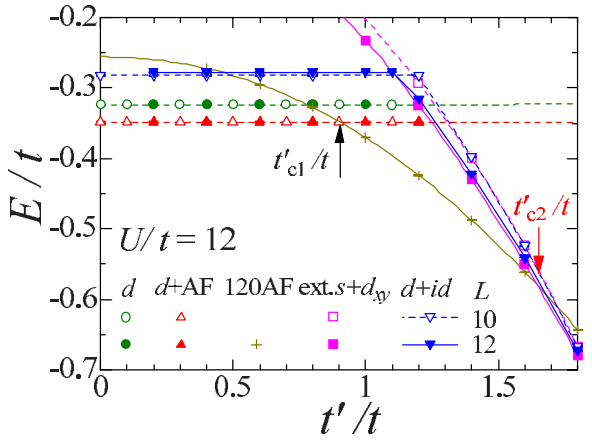

FIG. 4. (Color online) Comparison of total energies in the insulating regime ($U/t=12$) as a function of t'/t among various states: a coexisting state $\Psi_Q^{\rm co}$ [d+AF], a 120°-AF state Ψ_Q^{120} [120 AF], and three singlet states: a d wave Ψ_Q^{d} [d], an ext.$s+d_{xy}$ wave $\Psi_Q^{s+d'}$ [ext.$s+d_{xy}$], and a $d_{x^2-y^2}+id_{xy}$ wave Ψ_Q^{d+id} [$d+id$]. The latter two states will be discussed in Sec. III D. The arrows indicate the boundary values between t_c'/t and t_{c2}'/t, satisfying $E^{120}=E^{\rm co}$ and $E^{120}=E^{s+d'}$, respectively.

$$E_c = E^F - E, \tag{17}$$

where E^F denotes the energy per site of the projected Fermi sea, $\Psi_Q^F=\mathcal{P}\Phi_F$, as the reference value. In Fig. 5, $E_c^{\rm co}$, E_c^{120}, and E_c^{d} are shown for three values of t'/t. Note that E_c for every state is almost zero for $U<U_c^{\rm min}$, where $U_c^{\rm min}/t$ is shown by an arrow in each panel. This means that every state for $U<U_c^{\rm min}$ is almost reduced to a normal metallic state Ψ_Q^F. Here, it is important to recall that, as discussed in (I),[26] robust SC occurs only for $U_{\rm onset}^d<U<U_c^d$, in which E_c/t has a small but perceptible finite value. Although this tendency can be seen in E_c^d/t for $t'/t=0.6$ and $6\lesssim U/t<7.15$ [Fig. 5(a)], more stable $\Psi_Q^{\rm co}$ covers the whole range of SC, namely, $U_c^{\rm min}=U_c^{\rm co}<U_{\rm onset}^d$. Consequently, Ψ_Q^d comes to have no chance to arise appreciable SC. We will return to this subject in Sec. III B.

B. Metal-insulator transitions

In this subsection, we study the critical behavior at $U=U_c$ found in $E^{\rm co}$ and E^{120} (cusps) in Fig. 3, and in $E_c^{\rm co}$ and E_c^{120} (sudden increases) in Fig. 5. Although we have not mentioned, in fact, $E^{\rm co}$ and E^{120} in Fig. 3 undergo clear hysteresis (dual-minimum behavior) near the cusps at U_c. This indicates a kind of first-order transition takes place at U_c. We will reveal the properties of this transition with various quantities.

First, we take up the doublon density,

$$D = \frac{1}{N_s}\sum_i \langle n_{i\uparrow}n_{i\downarrow}\rangle = \frac{1}{N_s}\frac{\langle \mathcal{H}_{\rm int}\rangle}{U}, \tag{18}$$

where $\mathcal{H}_{\rm int}$ denotes the second (interaction) term of the Hamiltonian Eq. (1). D is regarded as the order parameter of metal-insulator transitions[27] by analogy with the particle density in gas-liquid transitions. As shown in Fig. 6, D exhibits a discontinuity at $U=U_c$ for each t'/t, strongly suggesting a first-order metal-insulator transition.

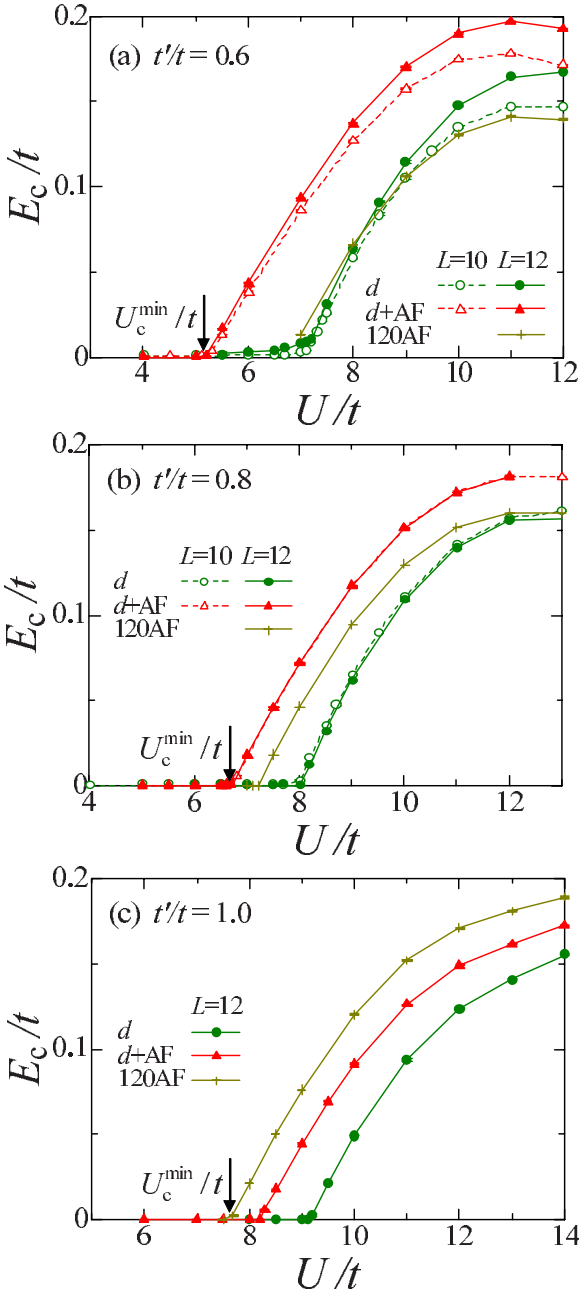

FIG. 5. (Color online) Comparison of the condensation energy E_c/t among $\Psi_Q^{\rm co}$ (d+AF), Ψ_Q^{120} (120 AF), and Ψ_Q^{d} (d) for (a) $t'/t=0.6$, (b) 0.8, and (c) 1.0. The arrow on the horizontal axis in each panel indicates the critical point of the metal-insulator transition arising at the smallest U_{rmc} ($\equiv U_{rmc}^{\rm min}$) among those states.

In Fig. 7, the momentum distribution function,

$$n(\mathbf{k}) = \frac{1}{2}\sum_\sigma \langle c_{\mathbf{k}\sigma}^\dagger c_{\mathbf{k}\sigma}\rangle, \tag{19}$$

of the lowest-energy states is plotted for $t'/t=0.8$ ($\Psi_Q^{\rm co}$) and 1.0 (Ψ_Q^{120}). Discontinuities of $n(\mathbf{k})$ at $\mathbf{k}_F$ in both sections, $(0,0)$-$(0,\pi)$ and $(0,0)$-(π,π), are obvious for $U<U_c$ for

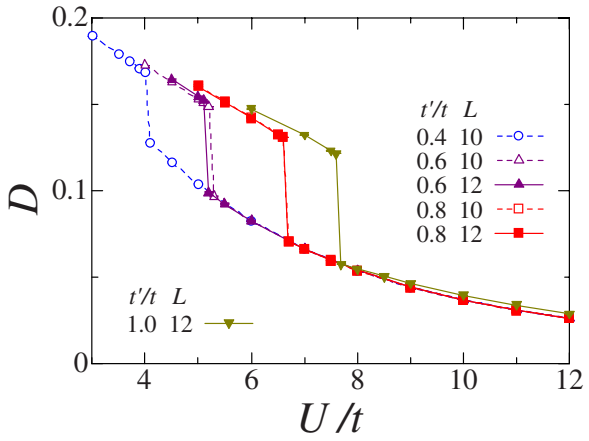

FIG. 6. (Color online) Density of doubly-occupied site (doublon) as a function of U/t for the lowest-energy states: the coexisting state Ψ_Q^{co} for $t'/t=0.4-0.8$ and the 120°-AF state Ψ_Q^{120} for $t'/t=1.0$.

both magnetic states, whereas $n(\mathbf{k})$ becomes smooth in both sections for $U>U_c$. Because the quasi-Fermi surface vanishes for $U>U_c$, we may consider that the state becomes nonmetallic.

In Fig. 8, we depict the charge structure factor,

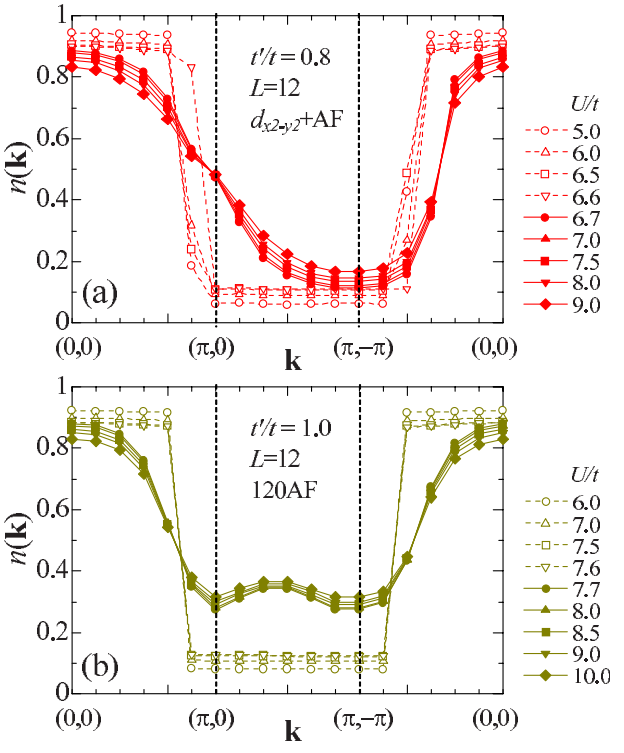

FIG. 7. (Color online) The momentum distribution function of the lowest-energy states is shown for various values of U/t along the path $(0,0)-(\pi,0)-(\pi,-\pi)-(0,0)$ in the Brillouin zone (a) for $t'/t=0.8$ (coexisting state Ψ_Q^{co}, $U_c/t\sim 6.65$) and (b) for $t'/t=1.0$ (120°-AF state Ψ_Q^{120}, $U_c/t\sim 7.65$). The open (solid) symbols denote the data for $U<U_c$ ($U>U_c$).

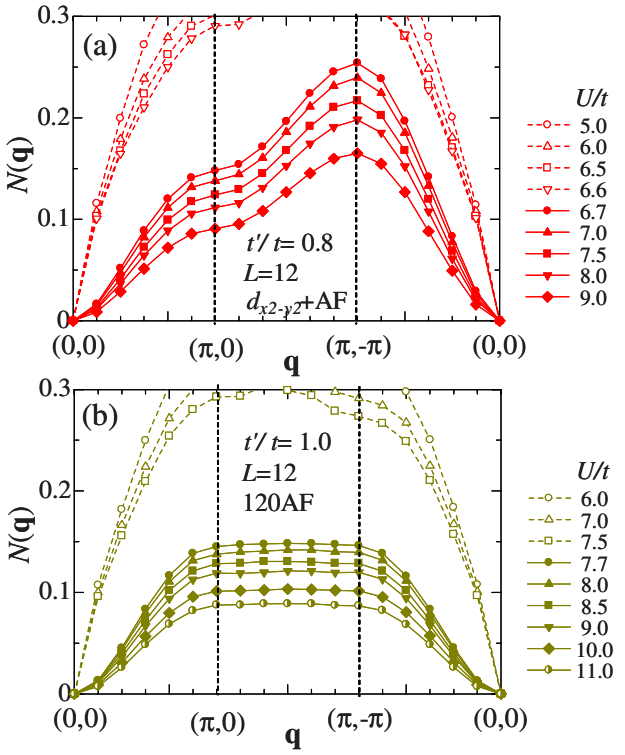

FIG. 8. (Color online) The charge structure factor $N(\mathbf{q})$ for the same states with those in Fig. 7 is plotted along the same path: (a) Coexisting state Ψ_Q^{co} for $t'/t=0.8$ and (b) 120°-AF state Ψ_Q^{120} for $t'/t=1.0$. The open (solid) symbols denote the data for $U<U_c$ ($U>U_c$).

$$N(\mathbf{q})=\frac{1}{N_s}\sum_{i,j}e^{i\mathbf{q}\cdot(\mathbf{R}_i-\mathbf{R}_j)}\langle N_iN_j\rangle-n^2, \tag{20}$$

with $N_i=n_{i\uparrow}+n_{i\downarrow}$ for the same states as those in Fig. 7. Similarly to the case of Ψ_Q^d studied in (I), $N(\mathbf{q})$ near the Γ point (0,0) seems linear in $|\mathbf{q}|$ for $U<U_c$, whereas the behaviors of $N(\mathbf{q})$ abruptly change to roughly quadratic in $|\mathbf{q}|$ for $U>U_c$, regardless of Ψ_Q^{co} or Ψ_Q^{120}. It follows that the states are gapless in the charge sector and are conductive for $U<U_c$, but a charge gap opens for $U>U_c$, and they become insulating.

The above results of D, $n(\mathbf{k})$, and $N(\mathbf{q})$ indicate that in Ψ_Q^{co} and Ψ_Q^{120}, a first-order metal-to-insulator transition occurs at $U=U_c$, as we showed for Ψ_Q^d in (I). Nevertheless, the quantities studied below will show that these transitions do not belong to pure Mott transitions with no relevance to magnetism like in Ψ_Q^d, but to metal-to-magnetic-insulator transitions.

Let us consider the optimized variational parameters in the correlation factor $\mathcal{P}$. Shown in Figs. 9(a)–9(c) is the U/t dependence of the optimized values of g, μ, and μ' for the lowest energy states: Ψ_Q^{co} for $t'/t=0.4-0.8$ and Ψ_Q^{120} for $t'/t=1.0$. The fact that all the parameters show apparent discontinuities at $U=U_c$ supports the first-order transition. In comparing these values with the corresponding ones for Ψ_Q^d shown in Fig. 4 in (I), we notice that the behavior of the Gutzwiller parameter g is opposite near the critical point. At $U=U_c$, g for Ψ_Q^{co} ($t'/t\leq 0.8$) becomes larger in the insulating

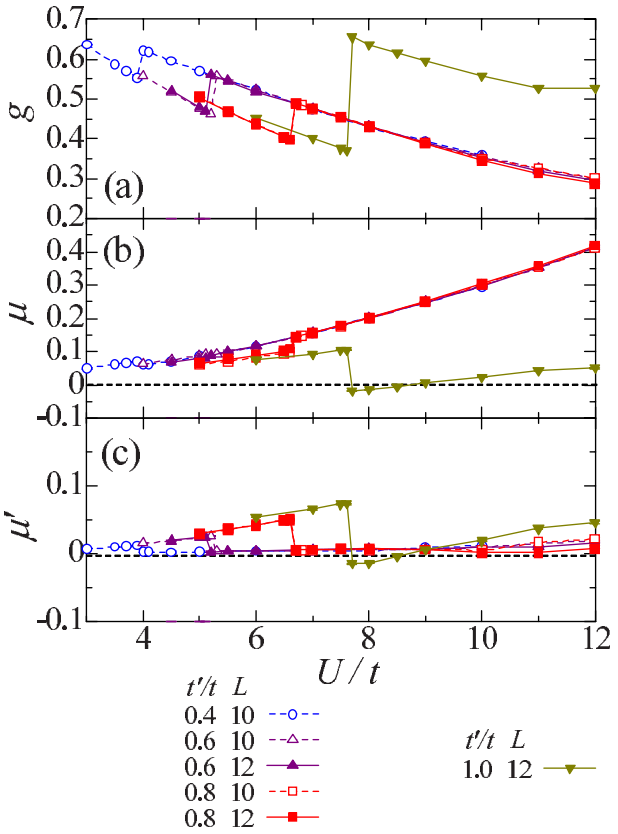

FIG. 9. (Color online) Optimized values of variational parameters in correlation factor $\mathcal{P}$ for several t'/t as function of U/t; (a) g [onsite (Gutzwiller) correlation parameter], (b) μ [doublon-holon binding parameter in the direction of t], and (c) μ' [the same of t']. For $t'/t=0.4-0.8$, the parameters are optimized in the coexisting state $\Psi_Q^{\rm co}$, and for $t'/t=1.0$ in the 120°-AF state Ψ_Q^{120}. The symbols are common to all panels.

side $U>U_c$ than in the metallic side Fig. 9(a), in contrast to the case for Ψ_Q^d Fig. 4(a) in (I). This behavior can be understood reasonably if the (π,π)-AF order arises in the insulating regime; it is known[28] that g becomes larger in a projected (π,π)-AF state than in the corresponding paramagnetic state because the one-body Hartree–Fock state $\Phi_{\rm AF}$ already includes an effect to suppress the double occupation in inducing staggered spin structure. For Ψ_Q^{120} $(t'/t=1.0)$, the increase of g at U_c is still larger than that of $\Psi_Q^{\rm co}$, meaning that the triplicate staggered field in Φ_{120} forms a firmer order for the isotropic case.

Another noticeable difference is the behavior of the doublon-holon binding parameter μ. The discontinuity of μ at U_c is an order of magnitude smaller in $\Psi_Q^{\rm co}$ than in Ψ_Q^d for $t'/t\leq 0.8$. This behavior is considered reasonable, again assuming the (π,π)-AF order in the insulating regime. As we studied before,[22] the doublon-holon binding effect is intrinsic in the Néel background of $\Phi_{\rm AF}$. Accordingly, μ in the correlation factor $\mathcal{P}_Q$ plays a minor role for the (π,π)-AF state. This tendency becomes more thorough for Ψ_Q^{120}; μ in Ψ_Q^{120}, inversely, drops to almost zero at U_c and remains very small for $U>U_c$. Similarly, μ' drops to almost zero at U_c for Ψ_Q^{120} and also for $\Psi_Q^{\rm co}$. Thus, the doublon-holon binding factor is almost useless for Ψ_Q^{120} in the insulating regime. However, in the insulating regime of Ψ_Q^{120}, doublons exist, as shown in Fig. 6, and we have confirmed in the records of Monte Carlo sweeps that a doublon almost necessarily sits in a nearest-neighbor site of a holon. This indicates that the one-body HF state Ψ_Q^{120} already has a sufficient doublon-holon binding effect for finite Δ_{120}. At any rate, the binding (and unbinding) of a doublon to a holon must be the essence of Mott transitions.

To directly confirm the existence of long-range magnetic orders for $U>U_c$, we next discuss the behavior of the gap parameters, $\Delta_{\rm AF}$ and Δ_{120}, and the order parameter m_s. For $\Psi_Q^{\rm co}$, the sublattice magnetization m_s is given, as usual, by

$$m_s=\frac{1}{N_s}\left|\sum_j e^{i\mathbf{K}\cdot\mathbf{R}_j}\langle S_j^z\rangle\right|, \tag{21}$$

with $S_j^z=1/2(c_{j,\uparrow}^\dagger c_{j,\uparrow}-c_{j,\downarrow}^\dagger c_{j,\downarrow})$. Similarly, we define m_s for Ψ_Q^{120} as

$$m_s^{120}=\frac{1}{N_s}\left|\sum_j e^{i\mathbf{K}\cdot\mathbf{R}_j}\langle S_j^{Tz}\rangle\right|, \tag{22}$$

with $S_j^{Tz}=1/2(a_{j,\uparrow}^\dagger a_{j,\uparrow}-a_{j,\downarrow}^\dagger a_{j,\downarrow})$. For $m_s^{120}>0$, Ψ_Q^{120} has a 120°-AF order. In Figs. 10(a) and 10(b), we show $\Delta_{\rm AF}$ and m_s of $\Psi_Q^{\rm co}$ for three values of t'/t (≤ 0.8). The behavior of these two quantities is similar; they are negligibly small for $U<U_c$, whereas they abruptly increase at $U=U_c$ and preserve the large magnitude for $U>U_c$. They are almost independent of the value of t'/t. We will turn to this point in Sec. III C. Shown in Figs. 10(c) and 10(d) are Δ_{120} and m_s^{120} of Ψ_Q^{120} for $t'/t=1.0$. Their U/t dependence is basically the same as those of $\Psi_Q^{\rm co}$, but the magnitude of Δ_{120}/t and m_s^{120} is larger than that of $\Delta_{\rm AF}/t$ and m_s. In this point, the 120-degree AF order is not less steadfast than the (π,π)-AF order. The spin structure factor $S(\mathbf{q})$ is also checked (not shown), which has a sharp peak at $\mathbf{q}=(2\pi/3,2\pi/3)$ in the insulating regime of Ψ_Q^{120}, supporting the realization of the 120° spin structure. Thus, we have confirmed that a firm magnetic long-range order always arises in the insulating regime at least for $t'/t\leq 1$.

Finally, we discuss the d-wave gap Δ_d and the d-wave SC correlation function of the nearest-neighbor-site pairing:

$$P_d(\mathbf{r})=\frac{1}{4N_s}\sum_i\sum_{\tau,\tau'=\hat{\mathbf{x}},\hat{\mathbf{y}}}(-1)^{1-\delta(\tau,\tau')}\times\langle\Delta_\tau^\dagger(\mathbf{R}_i)\Delta_{\tau'}(\mathbf{R}_i+\mathbf{r})\rangle, \tag{23}$$

where $\hat{\mathbf{x}}$ and $\hat{\mathbf{y}}$ denote the lattice vectors in the x and y directions, and $\Delta_\tau^\dagger(\mathbf{R}_i)$ is the creation operator of a nearest-neighbor singlet,

$$\Delta_\tau^\dagger(\mathbf{R}_i)=(c_{i\uparrow}^\dagger c_{i+\tau\downarrow}^\dagger+c_{i+\tau\uparrow}^\dagger c_{i\downarrow}^\dagger)/\sqrt{2}. \tag{24}$$

Unless Δ_d increases, $P_d(\mathbf{r})$ does not increase, but the opposite does not hold, in contrast to the relation between $\Delta_{\rm AF}$ and m_s. It is possible that finite Δ_d indicates a non-SC singlet gap.[29] In contrast, $P_d(\mathbf{r})$ is a good indicator of $d_{x^2-y^2}$-wave SC and was studied in detail for Ψ_Q^d in (I), which yielded a conclusion that SC arises for $t'/t\leq 0.7$ within Ψ_Q^d. Here, we consider the long-distance behavior of $P_d(\mathbf{r})$ by $P_d^{\rm ave}$, which

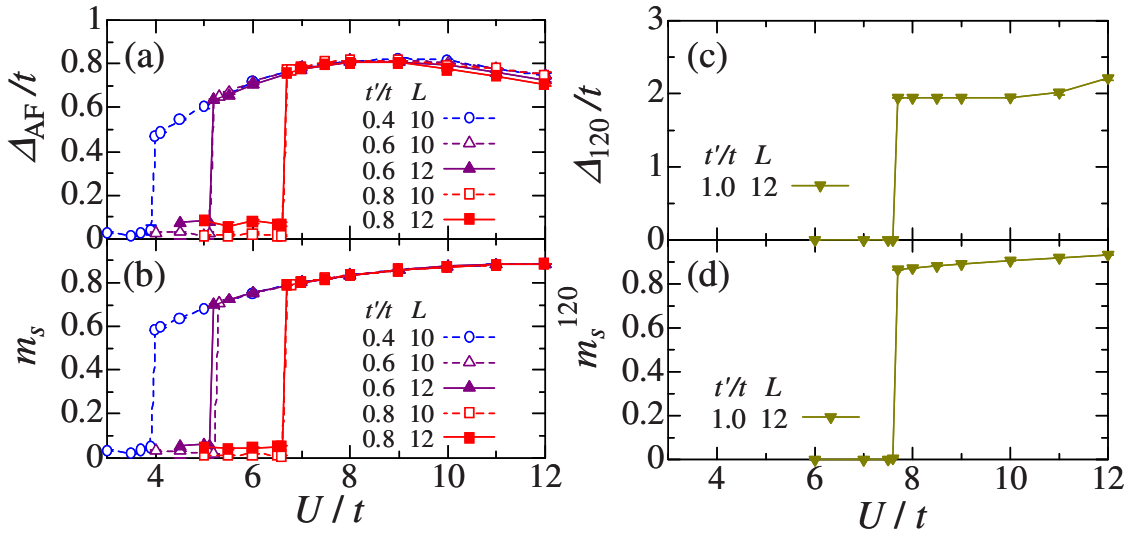

FIG. 10. (Color online) (a) Optimized gap parameter Δ_{AF}/t and (b) order parameter m_s of a (π,π)-AF order for the coexisting state Ψ_Q^{co} (t'/t=0.4–8). (c) Optimized gap parameter Δ_{120}/t and (d) order parameter m_s^{120} of a 120°-AF order for the 120°-AF state Ψ_Q^{120} (t'/t =1.0). For the full polarization, m_s and m_s^{120} become 1.

is the average of $P_d(\mathbf{r})$ only for $\mathbf{r}=(x,L/2)$ and $(L/2,y)$ with $x,y=0-L$.

As shown in Fig. 11(a), Δ_d for Ψ_Q^{co} is always substantially zero for $U<U_c$. Accordingly, $P_d(\mathbf{r})$ does not develop meaningfully, exceeding the value of $U=0$, even if U approaches U_c, as shown in Figs. 11(b) and 11(c). This is in contrast to the case of Ψ_Q^d. Thus, appreciable SC does not appear in the conducting regime. In the insulating regime, the d-wave singlet gap Δ_d is still strongly suppressed in Ψ_Q^{co} [Fig. 11(a)], compared with in Ψ_Q^d [Fig. 4(c)] in (I), where $\Delta_d/t \sim 1.2-1.3$. It is found, such as the case of Ψ_Q^d, $P_d(\mathbf{r})$ is very small and vanishes rapidly as L increases (not shown). Consequently, for $U>U_c$, the (π,π)-AF order is overwhelmingly dominant over the d-wave SC order; Ψ_Q^{co} in the insulating side can be regarded as an almost pure (π,π)-AF insulating state. It means that Ψ_Q^{co} undergoes a simple first-order metal-to-(π,π)-AF-insulator transition at $U=U_c$ (Ref. 30) for $t'/t \leq 0.8$.

In conclusion, there is no chance that robust d-wave SC or a nonmagnetic insulator appears within Ψ_Q^{co}.

C. Antiferromagnetic state and phase diagram

In this subsection, we consider the properties of the (π,π)-AF state realized in the insulating regime of Ψ_Q^{co}.

In (I), we found that the properties of Ψ_Q^d in the (nonmagnetic) insulating regime are almost independent of the frustration strength t'/t, cf. Fig. 4 for example. This tendency becomes more strong in Ψ_Q^{co}. As in Fig. 12(b), the renormalized frustration $\tilde{t}'/t$ becomes nearly zero for $U>U_c$, regardless of the model parameter t'/t, namely, in the strong coupling regime, the effective band almost retrieves the nesting condition for the simple square lattice ($t'=0$) even for highly frustrated cases.[31] The other variational parameters in Ψ_Q^{co} are also almost independent of t'/t, as seen in each panel of Figs. 9, 10(a), 11(a), and 12(a), where all the data points for $U>U_c$ are represented very well by a unique curve, regardless of t'/t. Thus, the optimized Ψ_Q^{co} is not changed with the frustration strength as long as $U>U_c$.

In Fig. 4, the total energy for Ψ_Q^{co} in the insulating regime (U/t=12) is plotted as a function of t'/t. Here, E^{co} is almost constant, and the difference of E/t between t'/t=0 and 1.2 is as small as 0.1%. This behavior is not trivial even if the wave function is not changed with t'/t because the t' term in the

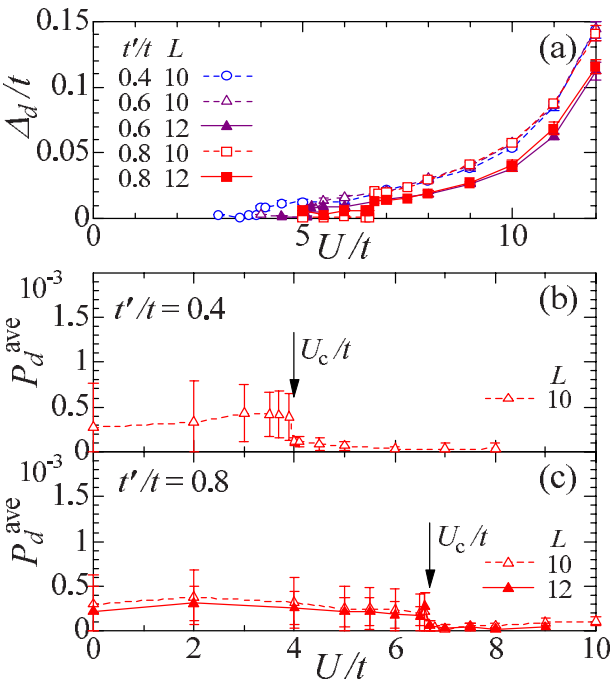

FIG. 11. (Color online) (a) Optimized values of d-wave gap parameter in Ψ_Q^{co} for t'/t=0.4–0.8 as a function of U/t. Averaged nearest-neighbor d-wave pairing correlation function in Ψ_Q^{co} for (b) t'/t=0.4 and (c) t'/t=0.8. Note that we average $P_d(\mathbf{r})$ only for large values of $|\mathbf{r}|$ (see text). For U/t=0, we use analytic values. The error bars in (b) and (c) include the standard deviations both of VMC calculations and by averaging with respect to r.

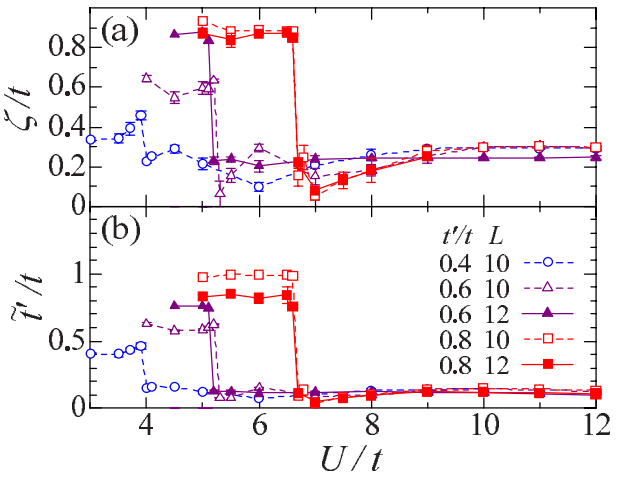

FIG. 12. (Color online) Optimized values of the remaining variational parameters in $\Psi_Q^{\rm co}$ for $t'/t=0.4-0.8$ as a function of U/t; (a) ζ/t [chemical potential] and (b) $\tilde{t}'/t$ [band renormalization factor]. The symbols are common in both panels.

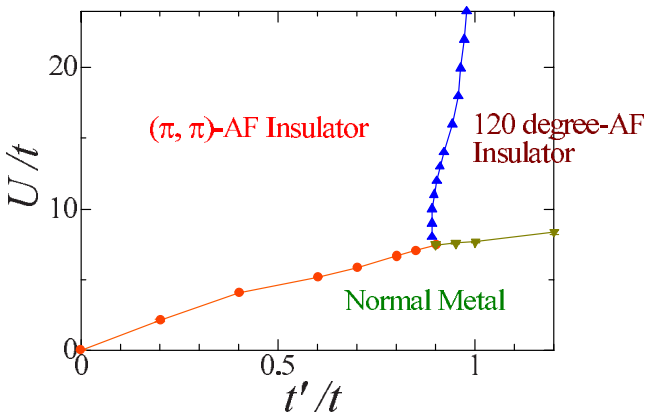

FIG. 13. (Color online) Ground-state phase diagram in the t'-U plane constructed from the present VMC results of the coexisting wave function $\Psi_Q^{\rm co}$ and the 120°-AF state Ψ_Q^{120}. At the boundaries of the metallic and insulating phases, first-order magnetic transitions take place.

Hamiltonian changes.[32] To understand this result, we check the behavior of energy components; let E_t, $E_{t'}$, and E_U be the contributions from the hopping in the t bond and t' bond directions, and from the onsite interaction U, respectively. We list the numerical data for $t'/t=0.8$ in Table I as a typical example because each contribution is again almost constant as a function of t'/t. As expected, $E_{t'}$ is substantially zero, indicating if we allow the band renormalization, the wave function is by far stabilized by retrieving the nesting condition for the simple square lattice at the cost of the energy reduction due to the diagonal hopping or frustration even if t'/t is considerably large.

It is natural to guess that this renormalization readily occurs in $\Psi_Q^{\rm co}$ because the nesting condition is advantageous not only to the (π,π)-AF state but to the d-wave state, as discussed in (I). Anyway, in recalling the point (iv) itemized in Sec. II, we notice that the band renormalization effect, namely the recovery of nesting, is essential to stabilize the (π,π)-AF state, as well as the d-wave singlet state.[23]

Finally, we discuss the ground-state phase diagram, which is reconstructed within $\Psi_Q^{\rm co}$ and Ψ_Q^{120} and depicted in Fig. 13. As compared to the diagram by Ψ_Q^d and $\Psi_Q^{\rm AF}$ shown in Fig. 14 in (I), the area of the (π,π)-AF insulator extends to extremely large t'/t (>0.9) and to somewhat small U/t. In addition, the area of the 120°-AF insulator appears near the isotropic point $t'/t=1$. We consider these tendencies to be broadly consistent with the results for the J-J' model ($U/t=\infty$),[4] in which the domain of (π,π)-AF continues to $t'/t>0.8$. In Fig. 13, as U/t increases, the boundary value in t'/t between the (π,π)-AF and 120°-AF insulators tends to increase. This is probably because $\Psi_Q^{\rm co}$ is stabilized by the d-wave gap Δ_d, which rapidly increases for large U/t, as seen in Fig. 11(a). We consider that the above tendency of the boundary will be corrected by introducing an appropriate singlet gap also into Ψ_Q^{120}. As a result of the stabilization of magnetic phases, the domains of nonmagnetic insulating and of robust d-wave SC phases disappear, which occupy certain parts of the phase diagram made in (I) and also in recent studies of a variational cluster perturbation theory[7] and a cellular dynamical mean field theory.[8]

D. Extension of pairing-gap form

From the argument in Sec. III C, we expect a state yielding a gain in $E_{t'}$ to overcome $\Psi_Q^{\rm co}$ and Ψ_Q^{120} for large t'/t. In this subsection, we consider a couple of different pairing gaps, which seem suitable for $t'\gtrsim t$, in the projected BCS function.

One has a specific gap parameter to the t' direction ($\Delta_{d'}$), independent of Δ_s for the t direction,[33,34]

TABLE I. Energy components and total energy of $\Psi_Q^{\rm co}$ for three values of U/t in the regime of the (π,π)-AF insulator ($U>U_c$). Here, $t'/t=0.8$ ($U_c/t\sim 6.65$). The small system-size dependence is a characteristic of an (π,π)-AF state.[28] The digits in brackets indicate the errors in the last digits.

U/t	L	E_t/t	$E_{t'}/t$	E_U/t	E/t
10	10	−0.7761(6)	−0.0001(0)	0.3659(6)	−0.4103(1)
	12	−0.7759(9)	−0.0001(0)	0.3657(9)	−0.4103(1)
12	10	−0.6618(7)	−0.0002(0)	0.3134(7)	−0.3485(1)
	12	−0.6601(6)	−0.0001(0)	0.3119(6)	−0.3483(1)
14	10	−0.5749(5)	−0.0002(0)	0.2713(6)	−0.3038(1)
	12	−0.5738(5)	−0.0001(0)	0.2703(7)	−0.3035(1)

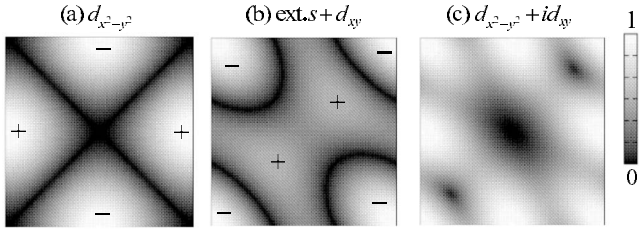

FIG. 14. Magnitude of pairing potentials $|\Delta_{\mathbf{k}}/\Delta_{\max}|$ considered in BCS state: (a) $d_{x^2-y^2}$, (b) ext.$s+d_{xy}$, and (c) $d_{x^2-y^2}+id_{xy}$. $|\Delta_{\max}|$ denotes the maximum of $|\Delta_{\mathbf{k}}|$ for each pairing gap.

$$\Delta_{\mathbf{k}} = \Delta_s(\cos k_x + \cos k_y) - \Delta_{d'} \cos(k_x + k_y), \tag{25}$$

which we call "ext.$s+d_{xy}$ wave" ($\Psi_Q^{s+d'} = \mathcal{P}\Phi_{s+d'}$). This form of $\Delta_{\mathbf{k}}$ has nodes near the k_x and k_y axes for $\Delta_s \sim \Delta_{d'}$ [see Fig. 14(b)], which resembles the nodes proposed by some experiments.[35,36] $\Delta_{\mathbf{k}}$ approaches the d_{xy} wave of a one-dimensional character for $|\Delta_{d'}| \gg |\Delta_s|$. The other is a $d_{x^2-y^2}+id_{xy}$ wave ($\Psi_Q^{d+id} = \mathcal{P}\Phi_{d+id}$),

$$\Delta_{\mathbf{k}} = \Delta_{d+id}[\cos k_x + e^{i2\pi/3}\cos(k_x + k_y) + e^{i4\pi/3}\cos k_y], \tag{26}$$

as shown in Fig. 14(c). This form was often used to study favorable gap symmetries for cobaltate SC;[37–39] using a VMC method[39] for the t-J model on an isotropic triangular lattice, it was shown that Ψ_Q^{d+id} is degenerate with Ψ_Q^d at half filling and has lower energy for doped cases. This gap form breaks time reversal symmetry.

In Fig. 4, the total energies of $\Psi_Q^{s+d'}$ ($E^{s+d'}$) and Ψ_Q^{d+id} (E^{d+id}) are plotted in addition to those mentioned earlier. For $t'/t \lesssim 1.1$, E^{d+id} is almost constant in the same reason as E^{co} and E^d, whereas E^{d+id} starts to decreases at $t'/t \sim 1.1$ abruptly because there, the direction of band renormalization is reversed from $\tilde{t}'/t \to 0$ to $\tilde{t}'/t \to \infty$. Thus, the effective Fermi surface of Ψ_Q^{d+id} becomes quasi-one-dimensional for $t'/t \gtrsim 1.1$. Similarly to E^{d+id}, $E^{s+d'}$ considerably decreases as t'/t increases. In the range of decreasing E, the energy reduction in both Ψ_Q^{d+id} and $\Psi_Q^{s+d'}$ is largely attributed to $E_{t'}$. Especially in $\Psi_Q^{s+d'}$, the energy reduction is entirely owed to $E_{t'}$, and the direction of band renormalization is $\tilde{t}'/t \to \infty$; the optimized Δ_s is negligible (~ 0.54) compared to the optimized Δ_L' (~ 7.05) for $U/t=12$, $t'/t=1.2$, and $L=12$. Thus, the singlet gap has an almost pure d_{xy} wave of one-dimensional character. As shown in Fig. 4, $E^{s+d'}$ overcomes E^{120} for $t' \gtrsim t'_{c2} \sim 1.65t$ for $U/t=12$, meaning that Ψ_Q^{120} is predominant for an unexpectedly large range of t'/t (>1), within the states we have studied ($L=10$ and 12). We expect a more favorable pairing gap will be found for $t < t' < t'_{c2}$, but we leave a search for it for the future.

Detailed results for $\Psi_Q^{s+d'}$ was reported in another publication.[40]

IV. CONCLUSION

A. Summary

As a continuation of the preceding study (I),[3] we have studied the Hubbard model on anisotropic triangular lattices, Eq. (1), at half filling using an optimization variational Monte Carlo method. We introduce two trial wave functions: (i) A coexisting state of (π,π)-AF and d-wave gaps, which allows for a band renormalization effect, Ψ_Q^{co}, and (ii) a state with an AF order of 120° spin structure, Ψ_Q^{120}. Main results are summarized as follows:

(1) First-order metal-to-insulator transitions occur in both Ψ_Q^{co} and Ψ_Q^{120} at smaller values of U/t than those of the d-wave state Ψ_Q^d studied in the preceding paper (I). As a result, the regime of robust d-wave SC found in (I) is covered with the domain of these states. The modified phase diagram within Ψ_Q^{co} and Ψ_Q^{120} is shown in Fig. 13.

(2) In the insulating regimes, Ψ_Q^{co} and Ψ_Q^{120} are considerably stable compared to Ψ_Q^d, and magnetic long-range orders always exist for $t'/t \lesssim 1.65$. Thus, a domain of a nonmagnetic insulator is not found for $t' \sim t$ within the wave functions used this time.

(3) In the insulating regime of Ψ_Q^{co}, the realized state can be regarded as a pure (π,π)-AF insulator because the sublattice magnetization, as well as the (π,π)-AF gap (Δ_{AF}), is robust, and the d-wave pairing correlation almost vanishes. In the optimized Ψ_Q^{co}, the effective band is renormalized so greatly ($\tilde{t}' \to 0$), irrespective of t'/t, that the nesting condition for $t'=0$ is retrieved almost completely. Accordingly, the contribution of diagonal hopping energy vanishes even for large t'/t.

(4) For $t' \sim t$, Ψ_Q^{120} becomes predominant ($U > U_c$) even though the effects of band renormalization and of coexisting singlet gaps are not considered. If these effects are introduced, the area of the 120°-AF order will somewhat expand, although at present, the area of the (π,π)-AF order extends to as large as $t'/t \gtrsim 0.9$.

(5) For large values of t' ($> t_{c2} \sim 1.65$), the singlet pairing states with gaps oriented to the diagonal-bond direction overcome Ψ_Q^{120}. We speculate that another predominant singlet (and SC) state will be discovered for $t < t' < t_{c2}$.

We believe that the mechanisms of a Mott (conductive-to-nonmagnetic insulator) transition and of the $d_{x^2-y^2}$-wave SC pursued in (I) fundamentally remain valid if the magnetic orders are removed for some reasons. However, the ground-state phase diagram for the model Eq. (1) is substantially modified by Ψ_Q^{co} and Ψ_Q^{120}.

B. Discussions

In comparing the present results with experimental ones of κ-ET salts, a favorable point is that a (π,π)-AF insulator is realized for realistic values of t'/t, namely, e.g., 0.74 in κ-$(\mathrm{ET})_2\mathrm{CuN}(\mathrm{CN})_2\mathrm{Cl}$. An unfavorable point is that robust SC and a nonmagnetic insulator do not appear; the latter state is believed to be realized in κ-$(\mathrm{ET})_2\mathrm{Cu}_2(\mathrm{CN})_3$.[10] One conceivable cause of this discrepancy is the insufficiency of trial wave functions; it is possible that quantum fluctuation is not sufficient for $U \sim U_c$ and large t'/t, and that we have not

exhausted crucial orders. Another possible cause is that the present model Eq. (1) is not sufficient to describe κ-ET salts. For instance, the dimerization of ET molecules is not strong enough to justify the use of a single-band model.[41]

In the theoretical point of view, the present result is comparable to that for $U/t \to \infty$, namely the J-J' Heisenberg model. According to it, the (π, π)-AF long-range order vanishes at $t'/t \sim 0.8$,[4] and an AF order with 120° spin structure prevails at $t'/t=1$,[11] although a disordered phase may intervene between the two magnetic phases. Some other theoretical studies[5,7–9] for the equivalent Hubbard model have yielded results of nonmagnetic insulating states at $t'/t \sim 1$. However, these studies have not explicitly treated the 120°-AF order, which is shown very stable for $t'/t=1$ in this study.

Although robust SC does not appear within the present study, we found that the symmetry of a singlet gap changes at large t'/t (~ 1.2) from the simple $d_{x^2-y^2}$ wave to, for instance, the d_{xy} wave as mentioned in Sec. III D (see Fig. 4). This aspect is in accordance with that of FLEX,[42] in which a predominant SC symmetry switches from a $d_{x^2-y^2}$-wave to a d_{xy}-wave state at $t'/t \sim 1$. Owing to this competition between $d_{x^2-y^2}$ and d_{xy} waves near the isotropic point ($t'/t=1$), the SC gap symmetry realized in κ-ET salts, especially in κ-$(ET)_2Cu_2(CN)_3$, may not be definitive but sensitive to physical parameters such as pressure. In contrast, a recent study of the Hubbard model with an extra exchange term using a Gutzwiller approximation[43] concluded that a $d+id$-wave SC is stable for $U \sim W$ and $t' \gtrsim t$. Thus, it is urgent to carry out VMC calculations, in which the form of the pairing gap can be optimized without biased assumptions.

ACKNOWLEDGMENTS

The authors appreciate the useful communication with Yung-Chung Chen, who has independently pointed out the importance of the renormalization of $\varepsilon_{\mathbf{k}}$ for the AF phase.[44] The authors thank Masao Ogata and Kenji Kobayashi for useful discussions. This work is partly supported by Grant-in-Aids from the Ministry of Education, Culture, Sports, Science and Technology, from NAREGI Nanoscience Project of the same Ministry, from the Supercomputer Center, ISSP, University of Tokyo and for the 21st Century COE "Frontiers of Computational Science."

[1] H. Kino and H. Fukuyama, J. Phys. Soc. Jpn. **65**, 2158 (1996).
[2] For recent reviews, see articles of Special Topics: Organic Conductors in J. Phys. Soc. Jpn. 75 (2006), Vol. 5.
[3] T. Watanabe, H. Yokoyama, Y. Tanaka, and J. Inoue, J. Phys. Soc. Jpn. **75**, 074707 (2006).
[4] W. Zheng, R. H. McKenzie, and R. P. Singh, Phys. Rev. B **59**, 14367 (1999); L. O. Manuel and H. A. Ceccatto, *ibid.* **60**, 9489 (1999).
[5] H. Morita, S. Watanabe, and M. Imada, J. Phys. Soc. Jpn. **71**, 2109 (2002).
[6] R. Zitzler, N.-H. Tong, Th. Pruschke, and R. Bulla, Phys. Rev. Lett. **93**, 016406 (2004).
[7] P. Sahebsara and D. Sénéchal, Phys. Rev. Lett. **97**, 257004 (2006).
[8] B. Kyung and A.-M. S. Tremblay, Phys. Rev. Lett. **97**, 046402 (2006).
[9] T. Koretsune, Y. Motome, and A. Furusaki, J. Phys. Soc. Jpn. **76**, 074719 (2007).
[10] Y. Shimizu, K. Miyagawa, K. Kanoda, M. Maesato, and G. Saito, Phys. Rev. Lett. **91**, 107001 (2003).
[11] B. Bernu, P. Lecheminant, C. Lhuillier, and L. Pierre, Phys. Rev. B **50**, 10048 (1994); L. Capriotti, A. E. Trumper, and S. Sorella, Phys. Rev. Lett. **82**, 3899 (1999).
[12] C. Weber, A. Laeuchli, F. Mila, and T. Giamarchi, Phys. Rev. B **73**, 014519 (2006).
[13] T. Giamarchi and C. Lhuillier, Phys. Rev. B **43**, 12943 (1991).
[14] A. Himeda and M. Ogata, Phys. Rev. B **60**, R9935 (1999).
[15] A. Himeda and M. Ogata, Phys. Rev. Lett. **85**, 4345 (2000).
[16] T. Watanabe, H. Yokoyama, Y. Tanaka, and J. Inoue, J. Magn. Magn. Mater. **310**, 648 (2007).
[17] M. C. Gutzwiller, Phys. Rev. Lett. **10**, 159 (1963).
[18] H. Yokoyama and H. Shiba, J. Phys. Soc. Jpn. **56**, 1490 (1987).
[19] H. Yokoyama and H. Shiba, J. Phys. Soc. Jpn. **59**, 3669 (1990).
[20] T. A. Kaplan, P. Horsch, and P. Fulde Phys. Rev. Lett. **49**, 889 (1982); P. Fazekas and K. Penc, Int. J. Mod. Phys. B **2**, 1021 (1988).
[21] H. Yokoyama, Prog. Theor. Phys. **108**, 59 (2002).
[22] H. Yokoyama, Y. Tanaka, M. Ogata, and H. Tsuchiura, J. Phys. Soc. Jpn. **73**, 1119 (2004).
[23] H. Yokoyama, M. Ogata, and Y. Tanaka, J. Phys. Soc. Jpn. **75**, 114706 (2006).
[24] W. F. Brinkman and T. M. Rice, Phys. Rev. B **2**, 4302 (1970).
[25] C. J. Umrigar, K. G. Wilson, and J. W. Wilkins, Phys. Rev. Lett. **60**, 1719 (1988).
[26] As studied in (Ref. 3), E_c^d for small t'/t ($\lesssim 0.7$) starts to increase gradually at $U \sim U_{\mathrm{onset}}^d$ ($< U_c^d$), as seen also in Fig. 5(a) (in this case $U_{\mathrm{onset}}^d/t \sim 6$). This increase stems from the SC gap opening. On the other hand, such increase cannot be seen in E_c^{co}, for arbitrary t'/t. This strongly suggests that robust SC is unlikely to arise in Ψ_Q^{co}.
[27] M. J. Rozenberg, R. Chitra, and G. Kotliar, Phys. Rev. Lett. **83**, 3498 (1999).
[28] H. Yokoyama and H. Shiba, J. Phys. Soc. Jpn. **56**, 3582 (1987).
[29] F. C. Zhang, C. Gros, T. M. Rice, and H. Shiba, Supercond. Sci. Technol. **1**, 36 (1988).
[30] For $t'=0$, a continuous metal-to-AF-insulator transition takes place at $U=0$. It follows that the character of the transition changes from continuous to first-order at $t' \sim 0$.
[31] In some weak-correlation approaches (Ref. 32), band renormalization toward the direction of retrieving the nesting condition has been found *in the conducting regimes*. However, these are phenomena essentially different from the very large band renormalization *in the insulating regime* discussed in this paper. As seen in Fig. 12(b), the renormalization for $U < U_c$ is too small to

detect in the present study. Incidentally, similar large band renormalization in strongly correlated regimes ($U > U_c$) has been found for *d*-wave states (Refs. 3 and 33).

[32] Y. Yanase and K. Yamada, J. Phys. Soc. Jpn. **68**, 548 (1999); H. Kontani, K. Kanki, and K. Ueda, Phys. Rev. B **59**, 14723 (1999); T. Ogawa, H. Kohno, and K. Miyake, Physica B **312-313**, 525 (2002).

[33] J. Liu, J. Schmalian, and N. Trivedi, Phys. Rev. Lett. **94**, 127003 (2005).

[34] Y. Tanuma, Y. Tanaka, K. Kuroki, and S. Kashiwaya, Phys. Rev. B **66**, 174502 (2002).

[35] K. Izawa, H. Yamaguchi, T. Sasaki, and Y. Matsuda, Phys. Rev. Lett. **88**, 027002 (2001).

[36] T. Arai, K. Ichimura, K. Nomura, S. Takasaki, J. Yamada, S. Nakatsuji, and H. Anzai, Phys. Rev. B **63**, 104518 (2001).

[37] B. Kumar and B. S. Shastry Phys. Rev. B **68**, 104508 (2003); G. Baskaran, Phys. Rev. Lett. **91**, 097003 (2003); Q.-H. Wang, D.-H. Lee, and P. A. Lee, Phys. Rev. B **69**, 092504 (2004).

[38] M. Ogata, J. Phys. Soc. Jpn. **72**, 1839 (2003).

[39] T. Watanabe, H. Yokoyama, Y. Tanaka, J. Inoue, and M. Ogata, J. Phys. Soc. Jpn. **73**, 3404 (2004).

[40] T. Watanabe, H. Yokoyama, Y. Tanaka, and J. Inoue, Physica C **463-465**, 152 (2007).

[41] J. Schmalian, Phys. Rev. Lett. **81**, 4232 (1998); K. Kuroki, T. Kimura, R. Arita, Y. Tanaka, and Y. Matsuda, Phys. Rev. B **65**, 100516(R) (2002).

[42] H. Kondo and T. Moriya, J. Phys. Soc. Jpn. **73**, 812 (2004).

[43] J. Y. Gan, Y. Chen, and F. C. Zhang, Phys. Rev. B **74**, 094515 (2006).

[44] Y. C. Chen (private communication).